Supplementary Material 1

3D-Cell-Annotator technical details

1 Introduction

In this supplementary, we introduce the theoretical foundations for the methods used in the software. 3D-Cell-Annotator is based on an extended version of active contours called selective active contour model [1]. The selective active contour model introduces two different priors, the *volume* and the *shape* prior; these priors are proposed in 3D-Cell-Annotator to extract single cells from clusters. Two different data terms are tested, the first one is the simplest *anisotropic edge detector* while the other one, called the *local region* data term, considers the environment of the contour to find the boundary of the object more effectively. The implementation uses the level set framework that naturally handles the topological deformations of the contour. Since one of the most fundamental limitations of the level set method is its numerical instability, we proposed a new method called *balanced phase field model*, that regularizes the level set in a *narrow band* in every iteration step to achieve numerical stability during the segmentation [2]. We briefly discuss both models here since these are the main building blocks of the algorithm used by the proposed software.

2 Selective active contours in 3D

The 2D selective active contour model was introduced to segment objects by considering their size and shape [1, 3]. We chose the level set framework because it is a powerful method for implementing interfacial problems like active contours [4].

2.1 Notations

Surfaces are denoted by $\mathbf{S} \subseteq \mathbb{R}^3$ or $\mathbf{S}(u, v) \in \mathbb{R}^3$ in parameterized form, where u and v are surface parameters. $\mathbf{S}_u(u, v), \mathbf{S}_v(u, v) \in \mathbb{R}^3$ are partial derivatives wrt. surface parameters (u,v), providing local (covariant) basis for the vectors of the tangent plane at $\mathbf{S}(u, v)$. Recall that $\mathbf{S}_u \times \mathbf{S}_v$ is normal to the surface. Assuming $\mathbf{S_u}, \mathbf{S}_v \mathbf{n}$ constitute a right handed basis, the inward pointing unit normal $\frac{\mathbf{S}_u \times \mathbf{S}_v}{|\mathbf{S}_u \times \mathbf{S}_v|}$ is denoted by $\mathbf{n}$. The sum curvature of the surface is denoted by K, while K_G is the Gaussian curvature. The integral $\int dS = \int \sqrt{|\mathbf{S}_u|^2 |\mathbf{S}_v|^2 - (\mathbf{S}_u \cdot \mathbf{S}_v)^2} du dv$ gives the surface area and $\int dV = -\frac{1}{6} \int \mathbf{S} \cdot (\mathbf{S}_u \times \mathbf{S}_v) du dv$ gives the volume of a surface $\mathbf{S}$, where dS and dV are the surface and volume element respectively.

Level set functions are denoted by $\phi = \phi(t, \mathbf{x})$, where $t \in \mathbb{R}$ and $\mathbf{x} = (x_1, x_2, x_3) \in \mathbb{R}^3$ are the time and space variables, respectively. According to this, ϕ_t denotes the partial derivative with respect to the time and $\nabla\phi$ denotes the spatial gradient $\nabla\phi = (\phi_{x_1}, \phi_{x_2}, \phi_{x_3})$. The Hessian matrix of ϕ is denoted by $\mathbf{H}(\phi) = (\phi_{x_i x_j})_{1 \leq i,j \leq 3}$.

2.2 The selective functional

There are four terms included in the functional of the selective active contour model. Below we provide a concise summary. For the details, see the original paper [1].

2.2.1 Volume prior

The volume prior prefers objects having a certain size and it is denoted by V_0.

$$\mathcal{V}(\mathbf{S}) = \frac{1}{kV_0^k}\left(\int dV - V_0\right)^k \tag{1}$$

The k is an arbitrary integer. If it is 2 then the contour tries to have a volume of exactly V_0 while if it is 3, it has an inflection at V_0 therefore it prefers a volume of 0 except at V_0 where the term has no effect.

2.2.2 Shape prior

The shape prior penalizes the deviation of the current surface from the preferred shape p (*plasma* or *amoeba value*). The currently implemented shape prior is called *sphericity* in 3D-Cell-Annotator but essentially it is the surface/volume ratio of the surface that is calculated as $p = \frac{area^{\frac{3}{2}}}{volume}$. The plasma value is minimal for the sphere, that is $p = 3\sqrt{4\pi} \approx 10.6$. We normalize the prior to assign 1.0 to the sphere so the sphericity is given by $p - 9.6$.

The shape prior that considers the surface volume ratio is then:

$$\mathcal{S}(\mathbf{S}) = \frac{1}{2V_0^2}\left[\left(\int dS\right)^{\frac{3}{2}} - p\int dV\right]^2 \tag{2}$$

2.2.3 Smoothness term

A curvature based smoothness term is applied to prevent the instability of the surface called Euler elastica. For the details, consult the original paper [1].

$$\mathcal{E}(\mathbf{S}) = \frac{1}{2}\int K^2 dS, \tag{3}$$

where the K is the sum curvature of the surface at a given point.

2.2.4 Data term

Two different data terms are tested, but there is a wide range of possible ones to choose from. The first one is the simple edge detector:

$$\mathcal{D}_{\mathcal{E}}(\mathbf{S}) = \int \nabla I \cdot \mathbf{n} dS, \tag{4}$$

where the I is the image.

The second one is a region based data term. It considers the mean intensities in the rectangular prisms positioned both in the inner and the outer side of the surface. In our setting the functional maximizes the intensity difference between the inner and outer part. If this data term is used, then the algorithm has three more parameters that define the size of the region (width, height and depth).

$$\Phi(\mathbf{S}, \mathbf{n}) = \frac{1}{4pqr} \left(\int_{\Re^+} I(\mathbf{p}) dV - \int_{\Re^-} I(\mathbf{p}) dV \right), \tag{5}$$

where $dV = d\xi d\zeta d\eta$, $\xi \in [-p, p]$, $\zeta \in [-q, q]$ and $\eta \in [0, r]$. $\mathbf{p}$ is in the local coordinate system, therefore $\mathbf{p} = \mathbf{S} + \xi \mathbf{e_1} + \zeta \mathbf{e_2} + \eta \mathbf{n}$ as it is visualised in fig. (1).

Therefore, we can use the local region as a data term in the selective model:

$$\mathcal{D}_{\mathcal{R}}(\mathbf{S}) = \int \Phi(\mathbf{S}, \mathbf{n}) dS. \tag{6}$$
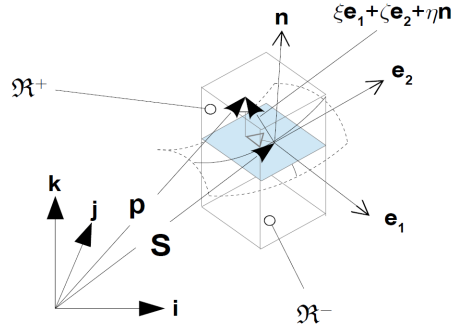

Figure 1: Visualisation of the local region in 3D. The local Cartesian coordinate system of the region is centered at the surface point $\mathbf{S}$ while the orientation is determined by the unit normal vector of the surface $\mathbf{n}$ and the unit basis vectors $\mathbf{e_1}, \mathbf{e_2}$ of the tangential plane of the surface.

2.2.5 Putting it all together: the composite functional

The composite functional therefore consists of the previously introduced terms and becomes the following:

$$\mathcal{L} = \alpha\mathcal{D} + \beta\mathcal{S} + \gamma\mathcal{V} + \delta\mathcal{E}, \tag{7}$$

where each term has an arbitrary real weight that can be controlled from the interface of the 3D-Cell-Annotator. The $\mathcal{D}$ can be either $\mathcal{D}_\mathcal{E}$ or $\mathcal{D}_\mathcal{R}$ depending on which data term is used.

2.3   The Euler-Lagrange equation for the functional

The extremal surface of the functional above can be found by solving the corresponding Euler-Lagrange equations. In our case (3D surfaces in the level set framework) they have the form:

$$|\mathbf{S}_u \times \mathbf{S}_v| Q\mathbf{n} = \mathbf{0}, \tag{8}$$

where Q is a scalar field with the functional derivatives: $Q = \alpha Q_{\mathcal{D}_\mathcal{E}} + \beta Q_\mathcal{S} + \gamma Q_\mathcal{V} + \delta Q_\mathcal{E}$.

That is, for the volume prior, we have $Q_\mathcal{V} = -\frac{1}{V_0^3}(\int dV - V_0)^2$ (V_0 is the target volume), for the shape prior (that takes sphericity into consideration) $Q_\mathcal{S} = \left[\left(\int dS\right)^{\frac{3}{2}} - p\int dV\right]\left[p - \frac{3}{2}K\left(\int dS\right)^{\frac{1}{2}}\right]$, p is the (unnormalized) target plasma value ($p = \frac{surface^{\frac{3}{2}}}{volume}$), for the data term, we have $Q_{\mathcal{D}_\mathcal{E}} = \Delta I$ and for the smoothness term we have $Q_\mathcal{E} = \frac{1}{2}K^3 - 2K_G K + \nabla \cdot \nabla K$, where K_G is the Gaussian curvature. The Euler-Lagrange of $\mathcal{D}_\mathcal{R}$ is slightly more complicated [3].

3   Level set regularization: the Balanced Phase Field model

3.1   Notations

In the level set framework, the representation of contours is given by a level set function of two variables $\phi(x, y)$. The quantities of the segmentation problem are extracted from this function, such as the unit normal vector $\mathbf{n} = \frac{\nabla\phi}{|\nabla\phi|}$ or the curvature $K = -\nabla \cdot \left(\frac{\nabla\phi}{|\nabla\phi|}\right)$ where ∇ is the gradient operator and "$\cdot$" stands for the scalar (dot) product, *i.e.* $\nabla \cdot \mathbf{v}$ is the divergence of the vector field $\mathbf{v}$.

3.2   From the phase field model to the balanced model

Since one of the fundamental problems of the level set method is its numerical instability, one should take care about the numerical errors by using some regularization method explicitly by not letting the active contour model to deform the level set from the signed distance function too much. We experienced severe issues with our selective model when we computed the curve evolution in level set framework, and the tested approximate solutions did not solve the issue,

while the more accurate methods made the algorithm too slow to be practical in reality. A simple observation is that maintaining the whole level set during the evolution is not necessary, since we always consider the derivatives in the neighborhood of the interface. Therefore it is enough to maintain the stability in this neighborhood called narrow band. Therefore we chose to apply a modified phase field solution to regularize the level set in every iteration. Using such a model, we treat the level set as a phase field, where the inner part of the contour is encoded with value 1 while the outer is with −1. Between the two, there is a *phase transition* with a necessary zero-crossing that models the contour. The goal is to maintain a smooth phase transition that is similar to the signed distance property of the level set near the contour. Furthermore, using the modified phase field model called balanced phase field, the authors do not only propose a solution to the numerical issues of the level sets but also eliminate the effect of the regularization method on the active model. In the following, we discuss the most important aspects of the model for the two dimensional case starting from the original phase field model and introducing the ideas behind the improved balanced phase field. For the details, and the intermediate steps of the derivation, consult [2].

In the original functional we had:

$$\int\int_\Omega \frac{D_0}{2}|\nabla\phi|^2 + \lambda_0\left(\frac{\phi^4}{4} - \frac{\phi^2}{2}\right)dA. \tag{9}$$

The solution of (9) is a scalar field ϕ with values ± 1 and a phase transition between the two values representing the narrow band of the contour. It is possible to embed the functional (9) to the active contour model directly by extending its functional with it, however it may lead to an extremely complex system considering its analysis. Instead of applying the phase field directly, one can use it in a shape maintenance role: before the next evolution step, the Euler-Lagrange equation associated with (9) can be solved independently, providing a regularized narrow band to the next iteration step.

However, a careful analysis shows that applying this functional to the level sets has a serious side effect on the active model by producing a curvature driven motion. In order to fix this issue, a Laplacian smoothness term is introduced and the original functional becomes the following:

$$\int\int_\Omega \frac{D}{2}(\Delta\phi)^2 + \lambda\left(\frac{\phi^4}{4} - \frac{\phi^2}{2} + \frac{1}{4}\right)dA. \tag{10}$$

However the proposed functional (10) still has a curvature dependent term and therefore produces the same effect when applied. It was shown that by using the combination of the smoothness terms from the previous functionals in a new one, with appropriate choice of the relative weights, the curvature dependency can be almost fully eliminated [2]. The new functional then becomes the following:

$$\int\int_\Omega \frac{D}{2}|\Delta\phi|^2 - \frac{D_0}{2}|\nabla\phi|^2 + \lambda\left(\frac{\phi^4}{4} - \frac{\phi^2}{2} + \frac{1}{4}\right)dA. \tag{11}$$

The conditions needed to be satisfied in order to cancel the effect of the curvature in the functional (11) depend on the width of the phase transition (w):

$$\lambda w^4 - 24D_0 w^2 - 720D = 0, \tag{12}$$

and

$$-D_0 \frac{3}{w} + D \frac{48}{w^3} = 0. \tag{13}$$

In order to satisfy the conditions (12) and (13), one should compute the parameters of (11) as a function of the desired width of the phase transition. Therefore we first should determine the width of the phase transition needed. This depends on the highest order of derivatives (n) used in the active model since we have to consider at least $n + 1$ points around the contour if we use the central difference schemes. The phase transition is non-linear, but the deviation from the linearity of its innermost part is negligible. This near-linear part is confined to the immediate neighbors of zero level set with the extent about half the size of the width parameter. Therefore, assuming the n-neighbors are used to calculate the differential quantities of the contour (using finite differences scheme) we use width parameter 2n+1 to obtain accurate values. Then, solving the conditions above, for the remaining parameters we get:

$$D_0 = 1, D = \frac{w^2}{16}, \lambda = \frac{21}{w^2}. \tag{14}$$

The associated Euler-Lagrange functional with the parameters only depending on the width of the phase transition is:

$$\frac{w^2}{16}\Delta\Delta\phi + \Delta\phi + \frac{21}{w^2}\left(\phi^3 - \phi\right) = 0. \tag{15}$$

The (15) can be implemented as simply as applying a (4-th order linear) filter modified by a point-wise value of the nonlinear (cubic) term for the grid points of the phase field lattice.

4   Implementation details

We briefly discuss the implementation of the selective algorithm and the 3D-Cell-Annotator software.

4.1   The selective model with the balanced phase field reinitialization model

We solve the Euler-Lagrange equations in the level set framework, therefore the following quantities can be substituted:

$$\mathbf{S}_u \times \mathbf{S}_v \mapsto \nabla\phi, \quad \mathbf{n} \mapsto \frac{\nabla\phi}{|\nabla\phi|}, \tag{16}$$

while the curvatures are computed as:

$$K \mapsto -\nabla \cdot \frac{\nabla\phi}{|\nabla\phi|}, \quad K_G \mapsto |\nabla\phi|^{-4} \begin{vmatrix} \mathbf{H}(\phi) & \nabla\phi^T \\ \nabla\phi & 0 \end{vmatrix}. \tag{17}$$

For minimizing the functionals a simple gradient descent is used. The finite differences are used to compute the derivatives numerically.

4.2 The software

The selective model is targeted to the CUDA architecture in C++. The level set values are only computed where the surface is located in the current iteration. The algorithm is distributed as a shared library and a new tool is created in the MITK that implements the communication between the shared library and the MITK.

References

[1] J. Molnar, E. Tasnadi, B. Kintses, Z. Farkas, C. Pal, P. Horvath, and T. Danka. Active surfaces for selective object segmentation in 3d. In *2017 International Conference on Digital Image Computing: Techniques and Applications (DICTA)*, pages 1–7, Nov 2017.

[2] J. Molnar, E. Tasnadi, and P. Horvath. A balanced phase field model for active contours. In *Seventh International Conference on Scale Space and Variational Methods in Computer Vision (SSVM 2019)*, pages 1–7, 2019.

[3] J. Moinar, A. I. Szucs, C. Molnar, and P. Horvath. Active contours for selective object segmentation. In *2016 IEEE Winter Conference on Applications of Computer Vision (WACV)*, pages 1–9, March 2016.

[4] S. Osher and J. Sethian. Fronts Propagating With Curvature Dependent Speed: Algorithms Based on Hamilton-Jacobi Formulations. *Journal of Computational Physics*, 79(1):12–49, 1988.

Supplementary Material 2
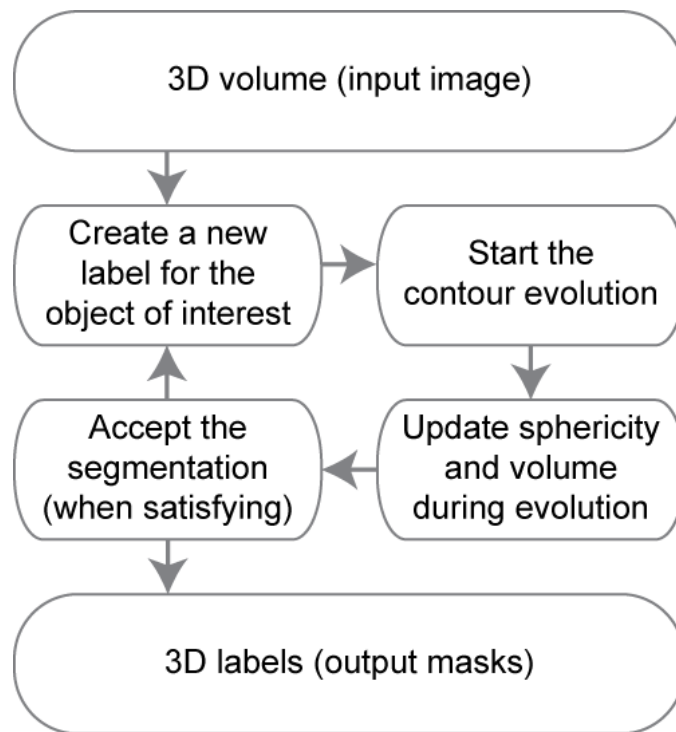
Figure. Flow-chart of the proposed segmentation approach. 3D-Cell-Annotator requires a 3D input image, typically a *z*-stack of sections acquired with a confocal/multiphoton/LSFM system. A label for each object is provided to start contour evolution. The surface immediately starts to evolve and the user may adjust some parameters (*e.g.* volume, sphericity) in real time. Finally, the obtained segmentation can be exported as a 3D binary mask.

Supplementary Material 3

All the datasets used in this work are publicly available and are described in other scientific papers:

1. The confocal dataset consists of 77 *z*-stacks containing a single-cell in each image stack. It was described by Poulet *et al.* 2014 and is publicly available at:
   https://www.gred-clermont.fr/media/WorkDirectory.zip

2. The LSFM dataset represents a small multicellular spheroid of 52 cells, used in Gole et al. 2016. It is publicly available under the name of "Neurosphere_Dataset" at:
   http://opensegspim.weebly.com/download.html

3. The confocal mouse embryo dataset contains 56 cells. It was used by Saiz et al. 2016. It is named "4May15FGFRionCD1_SU54_LM1.lsm" and it is publicly available in the native microscopy format (*i.e.* Zeiss ".lsm" format) at:
   https://figshare.com/articles/Raw_images_for_Saiz_et_al_2016/3767976/1
   In our analysis, we only dealt with blue channel of this dataset, i.e. the one related to nuclear staining.

Supplementary Material 4

The MATLAB (The MathWorks, Inc., MA, USA) code to compute the JI comparing 3D binary masks containing multiple objects, is available together with some utils at:

http://www.3d-cell-annotator.org/download.html

Note that during computation of JI, all the binary masks obtained with 3D-Cell-Annotator were dilated by a 1-pixel radius sphere to overcome the problem of active surface discretisation.

Supplementary Material 5

Table. Single-cell segmentation tools used in this work

	3D-Cell-Annotator (version 1.0)	MINS (version 1.3)	Pagita (version 2.2)	XPIWIT (version 1.0)	OpenSegSPIM (version 1.1)
DOCUMENTATION					
User guide	•	•	•	•	•
Website	•	•	o	o	•
Video tutorial	•	o	o	o	•
Freely available tool	•	•	•	•	•
Open source code	•	•	•	•	•
Implementation language	C++	MATLAB/C++	Java	C++	MATLAB
Test dataset/demo	•	•	•	•	•
Link to code/executable	www.3d-cell-annotator.org	http://katlab-tools.org	http://imagejdocu.tudor.lu	https://bitbucket.org/jstegmaier/xpiwit/downloads/	opensegspim.weebly.com
Scientific reference	Tasnadi et al., 2019	Lou et al., 2014	Gul-Mohammed et al., 2014	Bartschat et al., 2015	Gole et al., 2016
USABILITY					
No programming experience is required	•	•	o	o	•
User-friendly GUI	•	•	o	o	•
Intuitive visualization settings	•	•	o	o	o
No commercial license is required	•	•	•	•	•
Portability on Win/Linux/Mac	Win/Linux	Win	Win/Linux/Mac	Win/Linux/Mac	Win/Mac
FUNCTIONALITY					

Automatic single-cell segmentation	o	•	•	•	•
Manual correction opportunity	•	o	•	o	•
Feature extraction	o	•	•	•	•
No human interaction is required	o	o	o	o	o
OUTPUT					
3D rendering	•	o	o	•	o
3D binary mask	•	•	•	•	•
Features statistics	o	•	•	•	•

● available/yes; o not available/no

The above table compares the segmentations obtained with 3D-Cell-Annotator to other four publicly available tools. Hereafter we give a brief description of these tools.

1) MINS (version 1.3)
MINS stands for Modular Interactive Nuclear Segmentation, and it is a MATLAB/C++-based segmentation tool tailored for fluorescent intensity measurements of 2D and 3D image data. Today MINS (Lou *et al.* 2014) is one of the most widely used freely available tools for segmenting single-cells in embryos, but it can be easily used for 3D-oids as well. The MINS pipeline comprises three major cascaded modules: detection, segmentation, and cell position classification. Detection is based on a multiscale blob detection technique, and provides accurate localization of cell nuclei only. Segmentation expands detection output to cover the full nuclear body. The authors chose Seeded Geodesic Image Segmentation (SGIS) as the base algorithm for this stage. Finally, classification is obtained through a clustering-based approach combined with a robust shape-fitting approach and it serves multiple purposes, including the separation of multiple embryos and removal of outliers, as well as the classification of inner and outer cells. However, in practice, MINS requires only a few mouse clicks and a minimum of parameter tuning from the user. The source-code and a Windows-only standalone executable of MINS version 1.3 are distributed at: http://katlab-tools.org.

2) Pagita (version 2.2)
Pagita (Gul-Mohammed *et al.* 2014) is an automatic algorithm to segment and simultaneously classify cells/nuclei in 3D/4D images. Segmentation relies on training samples that are provided by the user through an iterative thresholding process. This algorithm can segment cells/nuclei even when they are touching, and remains effective under temporal and spatial intensity variations. However, it may be quite time-consuming since many threshold values are tested. The algorithm has been implemented as an open-source plug-in for ImageJ and is publicly available for download along with a tutorial and sample data at: http://imagejdocu.tudor.lu. The main idea of the algorithm is to use machine learning to improve the segmentation results. The learning step is an interactive process. The user first selects representative cells/nuclei by clicking on their locations inside the 3D or 4D dataset. The objects at the clicked positions are then segmented through an iterative thresholding procedure using the user-supplied volume estimates as a reference. Next, the user has to validate the proposed segmented nuclei, and 3D descriptors are computed from this set of validated nuclei. The main joint segmentation/classification procedure is subsequently applied to all time points.

3) XPIWIT (version 1.0)

XPIWIT (Bartschat *et al.* 2015) stands for XML Pipeline Wizard for ITK. It is an XML-based wrapper application for the Insight Toolkit that combines the performance of a pure C++ implementation with an easy-to-use graphical setup of dynamic image analysis pipelines. The core of XPIWIT is the Threshold of Weighted intensity And seed-Normal Gradient dot product image (TWANG) segmentation (Stegmaier *et al.* 2014). The current version of XPIWIT (*i.e.* version 1.0) incorporates about 70 different filters, and can be constantly extended with new functionality using the provided template files that facilitate the implementation of new modules. To apply a predefined XML processing pipeline to a desired set of images, XPIWIT has to be executed from the command prompt with command line input arguments. Alternatively, a configuration text file can be piped to the executable. This configuration file needs to contain the output path, one or more input paths, the path to the XML file to be processed, and may be customized using further optional parameters as described in the provided documentation. XPIWIT also has a GUI that allows to create and modify XML pipelines based on the filters compiled into the XPIWIT executable. XPIWIT has been successfully applied to segment and visualize terabyte-scale 3D+time light-sheet microscopy images of developing embryos. Its source-code, documentations and standalone versions are available at: https://bitbucket.org/jstegmaier/xpiwit/downloads/.

4) OpenSegSPIM (version 1.1)

OpenSegSPIM (Gole *et al.*, 2016) is an open-source and user-friendly 3D automatic quantitative analysis tool for confocal/multiphoton/LSFM data. It is a tool developed in MATLAB (The MathWorks, Inc., MA, USA). Its source-code, standalone versions (for Windows and Mac), documentation, user manuals and video tutorials are distributed at: http://opensegspim.weebly.com/. OpenSegSPIM assumes no prior knowledge of image processing or programming and is designed to easily segment nuclei/cells and compute several features without requiring human interaction, except for setting a few initial parameters: an approximate nuclei diameter measurement and intensity adjustment of the image contrast. OpenSegSPIM also includes: (a) a sub-cellular segmentation tool to analyse subcellular compartments, such as the cell membrane; (b) a simple post-processing tool for manually editing the segmentations obtained; and (c) an automatic batch process of time series and numerous datasets. However, the final segmentation of single-cells lacks quality, mainly due to the limits of thresholding in case of blurry objects and an improper separation of touching cells. The currently available version of OpenSegSPIM is version 1.1.

ADDITIONAL REFERENCES

(Bartschat, A. *et al.* 2015) Bartschat, A.; Hübner, E.; Reischl, M.; Mikut, R.; Stegmaier, J. (2015). XPIWIT-an XML pipeline wrapper for the Insight Toolkit. *Bioinformatics*, **32** (2), 315-317.

(Gul-Mohammed, J. *et al.* 2014). Gul-Mohammed, J.; Arganda-Carreras, I.; Andrey, P.; Galy, V.; Boudier, T. (2014) A generic classification-based method for segmentation of nuclei in 3D images of early embryos. *BMC Bioinformatics*, **15**(1), 9.

(Lou, X. *et al.* 2014). Lou, X.; Kang, M.; Xenopoulos, P.; Munoz-Descalzo, S.; Hadjantonakis, A.K. (2014). A rapid and efficient 2D/3D nuclear segmentation method for analysis of early mouse embryo and stem cell image data. *Stem cell reports*, **2**(3), 382-397.

(Stegmaier *et al.* 2014) Stegmaier, J.; Otte, J.C.; Kobitski, A.; Bartschat, A.; Garcia, A.; Nienhaus, G.U.; Strahle, U.; Mikut, R. (2014). Fast segmentation of stained nuclei in terabyte scale, time resolved 3D microscopy image stacks. *PLoS ONE*, **9**(2), e90036.

Supplementary Material 6

Single-cell dataset

To evaluate the segmentation quality of 3D-Cell-Annotator we used a dataset of 77 *z*-stacks, each containing a single cell. The masks obtained by 3D-Cell-Annotator were compared with manual "ground truth" segmentation. In order to obtain the ground truth for this dataset, we asked three expert annotators to segment the 77 *z*-stacks. For each stack we averaged their 3D segmentations by utilizing ReViMS (Piccinini *et al.* 2017, De Santis *et al.* 2019), a 3D extension of STAPLE (Warfield *et al.* 2004). We segmented the cells in a semi-automatic way by manually initializing with three contours on the three orthogonal axes, and then visually adjusting the parameters during surface evolution. The time spent by each human annotator on manually segmenting the 77 *z*-stacks was approximately 8 hours, whilst the time needed to obtain the same segmentations with 3D-Cell-Annotator was around 4 hours. The average JI between the expert annotators was 0.76. The JI between the annotators' average segmentations and 3D-Cell-Annotator was 0.77. The accuracy of 3D-Cell-Annotator reaches the level of an expert human annotator. The JI values calculated for each *z*-stack are reported in **Supplementary Material 7**.

Spheroid and embryo datasets

To demonstrate the usability and accuracy of 3D-Cell-Annotator for the analysis of real multicellular aggregates, we used a spheroid dataset imaged with an LSFM. The spheroid is composed of 52 cells (Gole *et al.* 2016). We compared the segmentations presented by two expert annotators with those obtained using 3D-Cell-Annotator and other four freely available tools: MINS (Lou *et al.* 2014, Saiz *et al.* 2016), Pagita (Gul-Mohammed *et al.* 2014), XPIWIT (Bartschat *et al.* 2015), and OpenSegSPIM (Gole *et al.* 2016). A brief description of these tools is available in **Supplementary Material 5**. The considered masks are the same as the ones previously used in Gole, L. *et al.* (2016). The average JI for the comparison of the performance of human experts was 0.66; the average JI comparing 3D-Cell-Annotator to the human annotators separately was 0.68 and 0.69, respectively, whilst none of the other tools performed better than 0.57 (**Supplementary Material 8**). Thus, it can be concluded that 3D-Cell-Annotator outperforms the analysed tools and its accuracy reaches the level of human experts'. In order to confirm this latter claim, we tested the software on another publicly available dataset, namely on a dataset of a mouse embryo consisting of 56 cells. Two expert operators segmented the cells manually in approximately 6 hours, whilst the time needed to obtain the same segmentations with 3D-Cell-Annotator was 3 hours. The average JI between human experts was 0.78; between 3D-Cell-Annotator and both human annotators was 0.80 (**Supplementary Material 9**). Again, these results confirm that 3D-Cell-Annotator offers an accuracy level reaching that of a human expert.
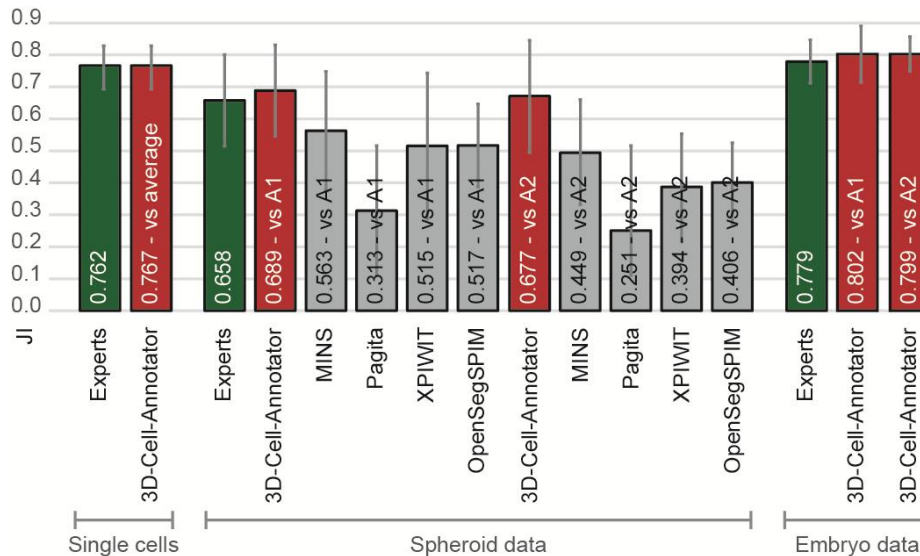

Figure. Summary of the Jaccard Indices (JI) computed by comparing the 3D masks obtained manually by human expert annotators, by four other freely available tools and by the proposed algorithm on the datasets shown in (Fig.1b), (Fig.1c) and (Fig.1d). 3D-Cell-Annotator outperformed every other software and reached an expert-like precision. A1 stands for *Annotator 1*; A2 for *Annotator 2*.

ADDITIONAL REFERENCES

(Bartschat, A. *et al.* 2015) Bartschat, A.; Hübner, E.; Reischl, M.; Mikut, R.; Stegmaier, J. (2015). XPIWIT-an XML pipeline wrapper for the Insight Toolkit. *Bioinformatics*, **32** (2), 315-317.

(De Santis, I. *et al.* 2019). De Santis, I.; Tasnadi, E.; Horvath, P.; Bevilacqua, A.; Piccinini, F. (2019). Open-source tools for volume estimation of 3D multicellular aggregates. *Applied Sciences*, **9**, 1616.

(Gul-Mohammed, J. *et al.* 2014). Gul-Mohammed, J.; Arganda-Carreras, I.; Andrey, P.; Galy, V.; Boudier, T. (2014) A generic classification-based method for segmentation of nuclei in 3D images of early embryos. *BMC Bioinformatics*, **15**(1), 9.

(Lou, X. *et al.* 2014). Lou, X.; Kang, M.; Xenopoulos, P.; Munoz-Descalzo, S.; Hadjantonakis, A.K. (2014). A rapid and efficient 2D/3D nuclear segmentation method for analysis of early mouse embryo and stem cell image data. *Stem cell reports*, **2**(3), 382-397.

(Piccinini, F. *et al.* 2017). Piccinini, F.; Tesei, A.; Zanoni, M.; Bevilacqua, A. (2017). ReViMS: Software tool for estimating the volumes of 3-D multicellular spheroids imaged using a light sheet fluorescence microscope. *BioTechniques*, **63**, 227-229.

(Stegmaier *et al.* 2014) Stegmaier, J.; Otte, J.C.; Kobitski, A.; Bartschat, A.; Garcia, A.; Nienhaus, G.U.; Strahle, U.; Mikut, R. (2014). Fast segmentation of stained nuclei in terabyte scale, time resolved 3D microscopy image stacks. *PLoS ONE*, **9**(2), e90036.

(Warfield, S.K. *et al.* 2004). Warfield, S.K.; Zou, K.H.; Wells, W.M. (2004). Simultaneous truth and performance level estimation (STAPLE): an algorithm for the validation of image segmentation. *IEEE transactions on medical imaging*, **23**, 903-921.

`

Supplementary Material 7

Table. Confocal dataset of 77 single-cell z-stacks: Jaccard Index (JI) values

	Annotator 1 vs Annotator 2	Annotator 1 vs Annotator 3	Annotator 2 vs Annotator 3	Annotators' average vs 3D-Cell-Annotator (semi-automatic modality)
SINGLE CELL JI				
	0.875	0.850	0.912	0.880
	0.873	0.844	0.894	0.868
	0.871	0.839	0.887	0.850
	0.868	0.838	0.876	0.848
	0.864	0.837	0.875	0.846
	0.864	0.833	0.870	0.846
	0.863	0.828	0.870	0.845
	0.859	0.822	0.868	0.844
	0.854	0.817	0.857	0.842
	0.853	0.808	0.854	0.840
	0.851	0.806	0.854	0.835
	0.851	0.804	0.851	0.832
	0.850	0.803	0.849	0.830
	0.849	0.801	0.847	0.830
	0.848	0.798	0.839	0.829
	0.848	0.785	0.836	0.828
	0.844	0.785	0.831	0.825
	0.844	0.782	0.831	0.823

0.844	0.779	0.830	0.822
0.842	0.776	0.828	0.820
0.839	0.768	0.822	0.820
0.838	0.759	0.822	0.816
0.836	0.757	0.820	0.812
0.834	0.755	0.818	0.810
0.833	0.754	0.817	0.808
0.832	0.750	0.816	0.801
0.831	0.743	0.814	0.799
0.828	0.743	0.809	0.796
0.824	0.739	0.808	0.796
0.824	0.738	0.805	0.795
0.823	0.738	0.803	0.794
0.820	0.737	0.801	0.791
0.819	0.736	0.799	0.789
0.818	0.735	0.798	0.785
0.815	0.732	0.796	0.785
0.814	0.727	0.796	0.782
0.814	0.726	0.795	0.782
0.809	0.723	0.789	0.780
0.808	0.722	0.788	0.780

0.805	0.719	0.788	0.778
0.804	0.716	0.784	0.777
0.799	0.701	0.781	0.772
0.794	0.700	0.776	0.766
0.793	0.698	0.775	0.765
0.787	0.694	0.775	0.762
0.785	0.693	0.772	0.761
0.784	0.689	0.767	0.747
0.783	0.685	0.767	0.746
0.781	0.681	0.765	0.743
0.778	0.681	0.765	0.741
0.776	0.679	0.764	0.738
0.776	0.675	0.761	0.737
0.768	0.671	0.760	0.737
0.768	0.669	0.757	0.735
0.760	0.664	0.757	0.733
0.757	0.663	0.753	0.730
0.751	0.653	0.745	0.724
0.744	0.652	0.744	0.723
0.744	0.652	0.742	0.717
0.743	0.645	0.737	0.712
0.742	0.643	0.735	0.710

0.742	0.636	0.735	0.709
0.739	0.635	0.726	0.707
0.736	0.631	0.723	0.704
0.733	0.630	0.712	0.698
0.726	0.626	0.712	0.697
0.724	0.613	0.709	0.696
0.720	0.609	0.701	0.678
0.697	0.604	0.700	0.676
0.686	0.599	0.699	0.676
0.680	0.598	0.698	0.674
0.673	0.595	0.698	0.661
0.668	0.574	0.693	0.654
0.647	0.570	0.683	0.649
0.644	0.558	0.680	0.647
0.643	0.536	0.646	0.643
0.627	0.532	0.640	0.610

AVERAGE ± STD

0.791±0.063	0.712±0.081	0.784±0.060	0.767±0.063

Supplementary Material 8

Table. Spheroid dataset: single-cell Jaccard Index (JI) values

	Annotator 1 vs Annotator 2	Annotator 1 vs 3D-Cell-Annotator	Annotator 2 vs 3D-Cell-Annotator	Annotator 1 vs MINS	Annotator 2 vs MINS	Annotator 1 vs Pagita	Annotator 2 vs Pagita	Annotator 1 vs XPIWIT	Annotator 2 vs XPIWIT	Annotator 1 vs OpenSegSPIM	Annotator 2 vs OpenSegSPIM
SINGLE CELL JI											
	0.887	0.889	0.900	0.856	0.722	0.840	0.834	0.745	0.625	0.735	0.696
	0.830	0.859	0.872	0.763	0.700	0.756	0.611	0.743	0.616	0.730	0.653
	0.819	0.837	0.855	0.763	0.667	0.747	0.577	0.718	0.609	0.703	0.584
	0.818	0.836	0.847	0.761	0.620	0.677	0.543	0.706	0.591	0.700	0.564
	0.789	0.822	0.837	0.733	0.610	0.659	0.474	0.704	0.588	0.693	0.554
	0.788	0.813	0.813	0.726	0.606	0.639	0.457	0.692	0.575	0.671	0.550
	0.784	0.813	0.806	0.724	0.606	0.533	0.435	0.690	0.572	0.660	0.532
	0.781	0.811	0.801	0.713	0.598	0.528	0.423	0.689	0.554	0.646	0.525
	0.781	0.811	0.799	0.709	0.583	0.464	0.365	0.689	0.552	0.640	0.518
	0.774	0.796	0.798	0.707	0.576	0.458	0.363	0.685	0.536	0.620	0.508
	0.774	0.782	0.797	0.688	0.574	0.442	0.360	0.676	0.533	0.620	0.505
	0.770	0.781	0.797	0.686	0.564	0.441	0.343	0.669	0.526	0.612	0.502
	0.760	0.779	0.794	0.685	0.549	0.441	0.317	0.666	0.524	0.608	0.500
	0.745	0.778	0.792	0.683	0.548	0.430	0.315	0.661	0.521	0.606	0.500
	0.741	0.776	0.788	0.678	0.540	0.427	0.314	0.658	0.521	0.605	0.496
	0.737	0.774	0.786	0.670	0.530	0.396	0.310	0.651	0.517	0.605	0.484
	0.729	0.766	0.784	0.666	0.527	0.394	0.305	0.644	0.517	0.602	0.484
	0.724	0.765	0.781	0.666	0.525	0.392	0.291	0.640	0.509	0.595	0.483

0.724	0.760	0.781	0.657	0.524	0.376	0.289	0.630	0.505	0.580	0.468
0.715	0.756	0.778	0.638	0.522	0.372	0.284	0.629	0.481	0.577	0.462
0.713	0.755	0.773	0.636	0.518	0.325	0.275	0.627	0.480	0.558	0.458
0.704	0.750	0.764	0.631	0.516	0.323	0.273	0.617	0.476	0.557	0.458
0.699	0.741	0.745	0.629	0.512	0.318	0.261	0.617	0.472	0.553	0.447
0.698	0.736	0.741	0.618	0.509	0.318	0.258	0.602	0.469	0.553	0.444
0.682	0.734	0.738	0.613	0.488	0.314	0.255	0.592	0.453	0.553	0.434
0.682	0.732	0.734	0.602	0.483	0.314	0.246	0.588	0.447	0.542	0.427
0.679	0.729	0.734	0.601	0.482	0.289	0.242	0.585	0.440	0.534	0.426
0.676	0.723	0.734	0.597	0.478	0.289	0.232	0.585	0.439	0.514	0.424
0.672	0.723	0.709	0.586	0.477	0.267	0.220	0.582	0.435	0.513	0.382
0.665	0.719	0.704	0.586	0.473	0.256	0.210	0.580	0.429	0.502	0.372
0.660	0.718	0.698	0.581	0.453	0.233	0.208	0.575	0.415	0.501	0.367
0.659	0.713	0.696	0.578	0.444	0.231	0.195	0.571	0.414	0.487	0.356
0.654	0.702	0.695	0.573	0.438	0.228	0.174	0.563	0.404	0.483	0.355
0.652	0.694	0.690	0.571	0.427	0.190	0.174	0.561	0.400	0.472	0.350
0.650	0.688	0.680	0.566	0.423	0.187	0.165	0.560	0.399	0.471	0.347
0.636	0.688	0.675	0.564	0.419	0.182	0.163	0.535	0.392	0.463	0.329
0.635	0.670	0.605	0.549	0.405	0.168	0.156	0.518	0.390	0.459	0.325
0.623	0.667	0.595	0.531	0.394	0.163	0.148	0.517	0.369	0.454	0.321
0.621	0.663	0.579	0.512	0.394	0.140	0.130	0.517	0.343	0.452	0.320

0.619	0.644	0.560	0.497	0.376	0.135	0.113	0.517	0.341	0.447	0.316
0.580	0.643	0.556	0.490	0.366	0.131	0.106	0.506	0.324	0.417	0.312
0.578	0.610	0.551	0.444	0.342	0.128	0.106	0.504	0.315	0.411	0.301
0.576	0.607	0.549	0.417	0.328	0.124	0.090	0.313	0.280	0.409	0.294
0.568	0.547	0.549	0.404	0.317	0.105	0.087	0.239	0.055	0.404	0.284
0.567	0.511	0.543	0.394	0.311	0.105	0.082	0.063	0.042	0.376	0.282
0.555	0.487	0.542	0.362	0.296	0.101	0.075	0.048	0.029	0.349	0.277
0.454	0.465	0.538	0.329	0.268	0.098	0.072	0.045	0.027	0.335	0.250
0.446	0.413	0.498	0.308	0.265	0.095	0.052	0.031	0.025	0.327	0.209
0.425	0.356	0.330	0.301	0.042	0.071	0.038	0.030	0.014	0.324	0.202
0.276	0.338	0.321	0.026	0.019	0.031	0.026	0.014	0.011	0.263	0.199
0.214	0.321	0.156	0.000	0.009	0.004	0.005	0.005	0.000	0.236	0.190
0.212	0.316	0.015	0.000	0.005	0.000	0.000	0.000	0.000	0.158	0.081

AVERAGE
± STD

0.658±0.143	0.689±0143	0.677±0.175	0.563±0.185	0.449±0.164	0.313±0.203	0.251±0.167	0.515±0.228	0.394±0.189	0.517±0.130	0.406±0.126

Supplementary Material 9

Table. Embryo dataset: single-cell Jaccard Index (JI) values

	Annotator 1 vs Annotator 2	Annotator 1 vs 3D-Cell-Annotator	Annotator 2 vs 3D-Cell-Annotator
SINGLE CELL JI			
	0.852	0.881	0.771
	0.721	0.794	0.746
	0.771	0.881	0.762
	0.809	0.889	0.827
	0.836	0.893	0.856
	0.789	0.888	0.853
	0.845	0.874	0.665
	0.878	0.896	0.768
	0.831	0.869	0.871
	0.766	0.891	0.778
	0.789	0.871	0.830
	0.858	0.878	0.810
	0.875	0.909	0.826
	0.684	0.832	0.827
	0.802	0.761	0.841
	0.784	0.908	0.805
	0.820	0.849	0.802
	0.796	0.862	0.852

0.804	0.843	0.825
0.778	0.918	0.805
0.839	0.869	0.861
0.659	0.846	0.812
0.869	0.888	0.822
0.770	0.844	0.798
0.815	0.797	0.727
0.785	0.884	0.732
0.713	0.909	0.754
0.727	0.866	0.821
0.855	0.781	0.742
0.724	0.709	0.842
0.803	0.768	0.837
0.702	0.791	0.799
0.821	0.869	0.793
0.827	0.853	0.688
0.759	0.804	0.813
0.788	0.696	0.816
0.690	0.752	0.747
0.759	0.774	0.791
0.824	0.721	0.862
0.834	0.625	0.795

0.842	0.775	0.762
0.682	0.671	0.740
0.760	0.647	0.725
0.765	0.666	0.770
0.767	0.677	0.880
0.586	0.584	0.737
0.623	0.627	0.855
0.596	0.702	0.759
0.706	0.718	0.871
0.797	0.697	0.880
0.809	0.767	0.868
0.857	0.783	0.882
0.770	0.785	0.841
0.790	0.800	0.794
0.844	0.720	0.724
0.791	0.878	0.681

AVERAGE ± STD

0.779±0.068	0.802±0.088	0.799±0.054